



HAL
open science

Toward new proton exchange batteries based on ionic liquid electrolyte: Metal hydride electrode / electrolyte coupling

Nesrine Chaabene, J. Zhang, Mireille Turmine, E. Kurchavova, Vincent Vivier, F. Cuevas, M. Mateos, M. Latroche, J. Monnier

► To cite this version:

Nesrine Chaabene, J. Zhang, Mireille Turmine, E. Kurchavova, Vincent Vivier, et al.. Toward new proton exchange batteries based on ionic liquid electrolyte: Metal hydride electrode / electrolyte coupling. *Journal of Power Sources*, 2023, 574, pp.233176. 10.1016/j.jpowsour.2023.233176 . hal-04129101

HAL Id: hal-04129101

<https://hal.science/hal-04129101>

Submitted on 15 Jun 2023

HAL is a multi-disciplinary open access archive for the deposit and dissemination of scientific research documents, whether they are published or not. The documents may come from teaching and research institutions in France or abroad, or from public or private research centers.

L'archive ouverte pluridisciplinaire **HAL**, est destinée au dépôt et à la diffusion de documents scientifiques de niveau recherche, publiés ou non, émanant des établissements d'enseignement et de recherche français ou étrangers, des laboratoires publics ou privés.

Toward new proton exchange batteries based on ionic liquid electrolyte: metal hydride electrode / electrolyte coupling

N. Chaabene¹, J. Zhang¹, M. Turmine^{2,3}, E. Kurchavova^{2,3}, V. Vivier^{2,3}, F. Cuevas¹, M. Mateos¹, M. Latroche^{‡,1}, J. Monnier^{§,1}

1: Univ. Paris Est Créteil, CNRS, ICMPE, UMR 7182, 2 rue Henri Dunant, 94320 Thiais, France

2: Sorbonne Université, CNRS, Laboratoire de Réactivité de Surface UMR 7197, 4 Place Jussieu, 75005, Paris, France

3: Sorbonne Université, CNRS, Laboratoire Interfaces et Systèmes Electrochimiques, UMR 8235, 4 Place Jussieu, 75005, Paris, France

Abstract

The voltage of an alkaline electrolyte-based battery is limited by the narrow electrochemical stability window of water. As an alternative to water, protic ionic liquid (IL)-based electrolytes have shown excellent conducting properties as well as a wide electrochemical stability window, and can therefore be implemented in protonic batteries. In this work, we present the physicochemical properties of different ILs that have been selected for their potential use in protonic batteries; namely, one aprotic IL (1-ethyl-3-methylimidazolium acetate [EMIM][Ac]) mixed with acetic acid (Ac.A) as proton donor, two protic ILs, the pyrrolidinium formate [Pyr][F] and the pyrrolidinium acetate [Pyr][Ac] and mixtures with their parent acid or base. The electrochemical properties of an AB_5 -type compound as negative electrode in a half-cell configuration using these ILs as electrolyte are then reported. A discharge capacity of $221 \text{ mAh}\cdot\text{g}^{-1}$ was attained at C/40 regime with low charge/discharge overpotential. Moreover, stable cycling performance was obtained by using [Pyr][Ac] as IL, with an electroactivity window of 2.2 V enlarged compared to the one of KOH.

Keywords: Protic ionic liquid, metal hydride, proton batteries

[‡] We honour our very dear Michel Latroche who significantly contributed to this scientific project and suddenly passed away.

[§] Corresponding author: Judith.monnier@cnrs.fr

List of abbreviations

Abbreviation	Definition
Ac.A	Acetic Acid
Pyrr	Pyrrolidine
[Pyrr][Ac]	Pyrrolidinium Acetate
Ni-MH	Nickel-Metal Hydride
IL	Ionic Liquid
[EMIM][Ac]	1-Ethyl-3-Methylimidazolium Acetate
[Pyrr][F]	Pyrrolidinium Formate
EW	Electrochemical Window
LSV	Linear Sweep Voltammetry
CV	Cyclic Voltammetry
HER	Hydrogen Evolution Reaction

1. Introduction

Aqueous batteries such as alkaline Nickel-Metal Hydride (Ni-MH) batteries, are widely used in emergency lighting, electric tools, household appliances, toys, etc. They are also being exploited to manage energy stationary storage in intermittent renewable energy production (photovoltaic and wind power) and for mobility in most of the hybrid electric vehicles (Toyota, Honda, Ford, etc.) as well heavy-duty vehicles such as buses, trucks and urban trams [1,2]. These aqueous batteries guarantee high safety due to their non-flammability and their reliability in both mobile and stationary applications. They have affordable cost, great robustness, high volumetric energy density – although reduced by the electrochemical window of water, and long service life, mainly limited by corrosion phenomena of the electrodes in a highly concentrated alkaline environment [3]. A way to improve these batteries is therefore to get rid of the aqueous electrolyte to extend the electrochemical window (EW) in order to improve operating voltage and minimize corrosion processes.

Ionic liquids (ILs) are molten salts at room temperature with high thermal stability and relatively high ionic conductivity. Typically, they consist of an organic cation (*e.g.* alkylpyrrolidinium, alkylpyridinium, alkylammonium, alkylimidazolium, etc.) and an inorganic anion (such as halide, tetrafluoroborate, hexafluorophosphate, nitrate, sulfonate, etc.) or organic anion (*e.g.* carboxylate, alkylsulfonate, etc.) [4]. One of the main advantages of ILs is

that their physical and chemical properties can be tuned by mixing them with other compounds [5]. The use of ILs in organic chemistry, pharmacology as well as in electrochemistry has been widely explored [6–9]. Generally, they can be divided in two families: (i) aprotic and (ii) protic ionic liquids [10].

Concerning energy storage, recent works have mainly focused on aprotic ILs as electrolytes for Li-ion batteries with the aim to overcome the flammability of conventional organic electrolytes and increase their electrochemical stability window. Although the performances are very promising, both the price and the viscosity of these aprotic ILs remain limiting factors for their practical use [11,12]. Conversely, protic ILs are less expensive, and possess ionic conductivities higher than $1 \text{ mS}\cdot\text{cm}^{-1}$. They have been used as a solvent for the synthesis of nanostructured matrix electrodes [13] and as an electrolyte in supercapacitors or Li-ion batteries [14], the latter being currently under development. They can also be mixed with an acid or a related base to adjust the pH and thus optimize their interaction with positive and negative electrodes.

A recent work considers the use of IL as a novel electrolyte for aqueous Ni-MH batteries [15], with LaNi_5 -type alloy as active material of the negative electrode. The electrolyte was a mixture based of an aprotic IL, alkylmethylimidazolium acetate [EMIM][Ac] and acetic acid (Ac.A), leading to high proton conductivity. Thus, in the frame of this work, aprotic ILs were used, although they are quite expensive. Moreover, $\text{Ni}(\text{OH})_2$ positive electrode was used. This electrode works at a low potential as compared to the possibilities given by the extended electrochemical window (EW). Furthermore, study of a full cell configuration makes it difficult to understand the individual properties of the negative and positive electrodes toward the electrolyte. To pave the way towards a new generation of IL-based proton exchange batteries, a fundamental study is required to understand separately the behavior of the proposed electrode materials.

The objective of this paper is to establish the first milestone in this direction, by studying the cycling of a negative electrode in a protic IL. As a proof of concept of this coupling of IL and negative electrode material, this paper focuses on the coupling of AB_5 -type alloys (A = rare-earth, B = $3d$ transition metal such as Ni) currently used in the Ni-MH technology with two ILs, the pyrrolidinium formate [Pyrr][F] and the pyrrolidinium acetate [Pyrr][Ac]. Moreover, the mixtures of [Pyrr][Ac] with acetic acid (Ac.A) or pyrrolidine (Pyrr) were characterized and used.

The galvanostatic charge/discharge cycling of the negative electrode has been performed in these different media and compared to that in the aprotic IL [Emim][Ac] mixed with Ac.A and in aqueous 8.7 M KOH solution.

1 Experimental section

1.1 Chemicals and synthesis of ionic liquids

The negative electrode material is an industrial AB_5 -type alloy (A = rare-earth, B = 3d late transition metal) provided by SAFT. It is a single AB_5 phase compound. Commercial pyrrolidine (Sigma Aldrich, purity $\geq 99\%$), acetic acid (Carlo Erba, purity $\geq 99.8\%$), and formic acid (Carlo Erba, purity $\geq 99\%$) were used as received. The graphical structures of the two protic ILs [Pyr][F] and [Pyr][Ac] are presented in Fig. 1.

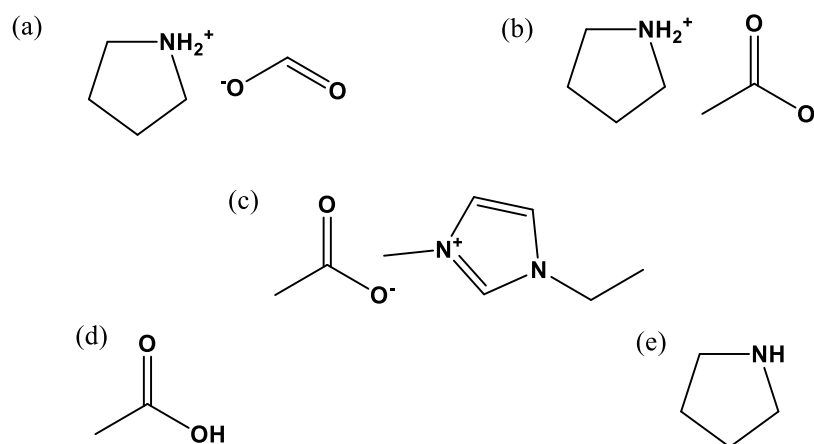


Figure 1: Graphical structures of ILs used in this work: a) [Pyr][F], b) [Pyr][Ac], c) [EMIM][Ac]. Some of them have been mixed with d) acetic acid or e) pyrrolidine

The synthesis of these two protic ILs was performed by mixing Pyr with a small quantity of water in a thermostatically controlled cell at $-10\text{ }^\circ\text{C}$. Then, a molar equivalent of formic or acetic acid was added dropwise in the cooled pyrrolidine under stirring. The synthesis was carried out at a temperature between $-10\text{ }^\circ\text{C}$ and $5\text{ }^\circ\text{C}$ in order to avoid any possible side reaction. After adding the acid, the solution was kept at low temperature under stirring for 24 h and then freeze-dried with a lyophilization machine (Operon FDU8606) to remove water. The synthesis of the ILs has been confirmed using ATR-FTIR spectroscopy (Figure S1a) and ^1H - and ^{13}C -NMR spectroscopy (Figure S1b). The residual amount of water in the two freshly prepared and freeze-dried ILs was titrated using a Karl Fisher coulometer (C20, Mettler Toledo). The water content of ILs varies depending on the synthesis between 0.5 and 5 wt.%.

Commercial aprotic IL, 1-ethyl-3-methylimidazolium acetate [EMIM][Ac], was purchased (Sigma Aldrich, purity $\geq 98\%$) in order to compare with the results of Meng *et al.* [15].

1.2 Electrochemistry and physicochemical analyses

Density measurements were performed using a vibrating-tube densimeter DMA 5000 M (Anton Paar) within the temperature range of 293 to 333 K. The apparatus was calibrated using the extended procedure with dry air and degassed ultra-pure water. All reported density data were corrected for the viscosity effect using the internal calibration of the densimeter. The sample was transferred to a syringe and injected into the densimeter. These measurements were performed with an uncertainty of less than $\pm 0.05 \text{ kg}\cdot\text{m}^{-3}$, whereas repeatability was estimated to be $\pm 0.005 \text{ kg}\cdot\text{m}^{-3}$. The temperature was measured with an uncertainty of $\pm 0.005 \text{ K}$ and a resolution of $\pm 0.001 \text{ K}$.

The viscosity was measured using a rolling-ball viscosimeter (Anton Paar – Lovis 2000M/ME) that is based on the concept of a falling ball inside a capillary of known diameter. The apparatus can be operated within a wide range of temperatures and angles. The measurements were performed with an uncertainty of less than 0.5%. The temperature of the capillary is controlled by a Peltier device within a precision of $\pm 10^{-3} \text{ K}$. A capillary tube of diameter 1.8 mm was used, allowing typically viscosity measurements between 13 to 300 mPa·s.

Ionic conductivity was measured using a CDM 230 Conductivity Meter (MeterLab, Radiometer analytical). The conductivity cell (Radiometer Analytical CDC741T-6) was equipped with a temperature sensor (2-pole Pt sensor, $K = 1.0 \text{ cm}^{-1}$, glass body). The experimental cell was calibrated with standard $0.1 \text{ mol}\cdot\text{L}^{-1}$ KCl solution prior to use. The measurements were performed with an uncertainty of 1%, and the temperature of the samples was controlled using cryothermostat polystat with thermal stability of $\pm 0.03 \text{ K}$.

The electroactivity window measurements were performed with a deaerated three-electrode cell using a GAMRY REF600 potentiostat. A homemade gold microelectrode of 200 μm in diameter was used as working electrode and a platinum grid of $1 \times 1 \text{ cm}^2$ was used as counter electrode.

The reference electrode was based on an Ag/AgNO₃ electrode in a double junction compartment. It consisted of a silver wire immersed in a first junction containing a saturated solution of silver nitrate (AgNO₃) in each studied IL, with a sintered glass at the bottom. A second junction containing pure IL was used to prevent the working solution in the main electrochemical compartment from any contamination of ions (Ag⁺ and NO₃⁻) coming from the first junction containing the reference electrode. Before electrochemical measurements, the working electrode was carefully cleaned by electrochemical cycling in a 0.1 mol·L⁻¹ sulfuric acid aqueous solution by sweeping the potential between -1 and 1.3 V/SCE at 100 mV·s⁻¹ for 10 min.

Galvanostatic cycling with potential limitation (GCPL) experiment have been performed in a deaerated three electrode cell, using a Biologic VMP3 Multi Potentiostat. The counter electrode was a platinum grid, the reference electrode was an Ag/AgNO₃ electrode in IL with a double junction as described above. The working electrode was a composite electrode made of 90 wt.% of the industrial AB₅-compound as active material, 5 wt.% of carbon black to serve as electronic conductor and 5 wt.% of PTFE as binder. The composite is spread out in a sheet of 250 μm in thickness. The resulting tape is dried under vacuum overnight, then cut in two rectangles of 4 x 10 mm². Those rectangles are pressed on both sides of a nickel grid as the current collector, to form the negative electrode. The mass loading is around 100 mg·cm⁻².

To serve as a benchmark, all the electrochemical experiments have also been carried out in a 8.7 mol L⁻¹ KOH solution. In this case, a Hg/HgO reference electrode was used.

X-ray diffraction (XRD) was performed using a Bruker D8 ADVANCE diffractometer with Cu-K_α radiation, in a 2θ-range from 10 to 110° with a step size of 0.02°.

2 Results and discussion

2.1 Physicochemical properties

a. Density

The density, ρ , as a function of temperature for pure [Pyrr][F], [Pyrr][Ac], mixtures of [Pyrr][Ac]/Ac.A or [Pyrr][Ac]/Pyrr, and a mix of [EMIM][Ac]/Ac.A are summarized in Table 1 for values at room temperature and in Supplementary material Figure S2 and Table S1. The density depends on the nature of the anion and the cation composing the IL. For the same cation (Pyrr⁺), when the acetate ion is replaced by the formate anion, the density decreases.

It should be noted that [Emim][Ac], which is an aprotic IL, mixed with Ac.A has the highest density. From the dependence of density on temperature, the coefficient of thermal expansion, α , was also determined and is given in Table S2.

Table 1 : Density ρ , viscosity η , ionic conductivity σ_{iL} at 25°C, activation energy for viscosity E_{η} , activation energy for conductivity E_{σ} , and the electrochemical window (EW) for the different media. Pyrr. stands for pyrrolidine, i.e., the conjugated base of [Pyrr][Ac] and Ac.A. stands for acetic acid, the conjugated acid of [Pyrr][Ac].

Medium	ρ (g.cm ⁻³)	η (mPa.s)	E_{η} (kJ. mol ⁻¹)	σ_{iL} (mS. cm ⁻¹)	E_{σ} (kJ. mol ⁻¹)	EW (V)
[Pyrr][F]	1.08003	12.5	21.92	36.63	4.42	2.0
[Pyrr][Ac]	1.05425	34.1	30.21	9.20	11.58	2.2
[Pyrr][Ac] + Ac.A (2M)	1.06064	28.0	28.24	8.04	10.85	2.3
[Pyrr][Ac] + Pyrr (2M)	1.02791	21.1	27.34	8.96	9.03	2.4
[EMIM][Ac]+Ac.A (2M)	1.10086	50.9	31.51	5.72	15.85	3.0

Dynamic viscosity (Table 1 for room temperature data and all data in supplementary material Figure S3 and Table S3) impacts the transport properties of the medium. It significantly affects the diffusion of protons in the environment, which is directly related to the ionic conductivity. The comparison of the viscosity values η for [Pyrr][Ac], pure or mixed with 2 mol L⁻¹ of Ac.A or Pyrr shows that the addition of acid or base decreases the viscosity. The activation energy (E_{η}) - the energy barrier that must be overcome by the ions to move through the medium – has been determined through the Arrhenius-like relationship:

$$\ln(\eta) = \ln \eta_{\infty} + \frac{E_{\eta}}{RT} \quad (\text{Eq.1})$$

The evolution of the ionic conductivity (σ_{iL}) for the five studied media within the temperature range from 20 to 60 °C is reported on

Figure 2 and Table S4. As expected, the ionic conductivity increases with the temperature due to the increase of the ion mobility and the decrease of the viscosity. At room temperature (Table 1), all the ILs show ionic conductivity higher than 1 mS.cm⁻¹, considered as the critical value for an IL to be used as electrolyte. Fig. 2 shows that the addition of acid or base increases the ionic conductivity of the pure IL. The activation energy E_{σ} is also obtained from an Arrhenius law (Table 1 and Figure S4). Assuming a spherical shape with effective radius r_i ,

electrostatic charge z_i and molar concentration c_i for the ions, the ionic conductivity of the ion i can be written as described in Supplementary Information (See Eq. S5) [16].

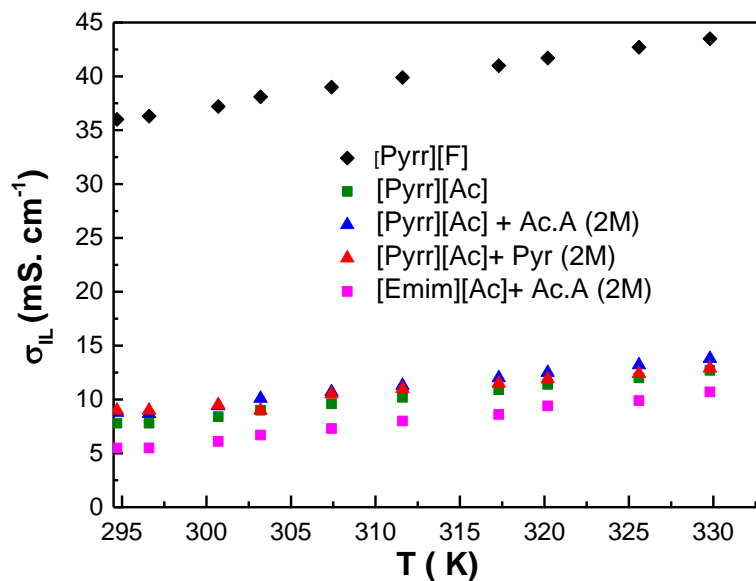


Figure 2 : Ionic conductivity measurements as a function of temperature within the range 20-60 °C for [Pyrr][F], [Pyrr][Ac], [EMIM][Ac] and [Pyrr][Ac] mixed with Ac.A or Pyr.

These physicochemical characterizations show that ILs and their mixtures with acid or base possess the required properties to be used as electrolytes. In addition, their EW is of outmost interest. It was determined by linear sweep voltammetry (LSV) with a 200 μm in diameter gold electrode at room temperature. The voltammograms for the five ILs at a scan rate of $5 \text{ mV}\cdot\text{s}^{-1}$ are presented on Figure 3, and are compared with a reference voltammograms performed in 8.7 KOH aqueous solution.

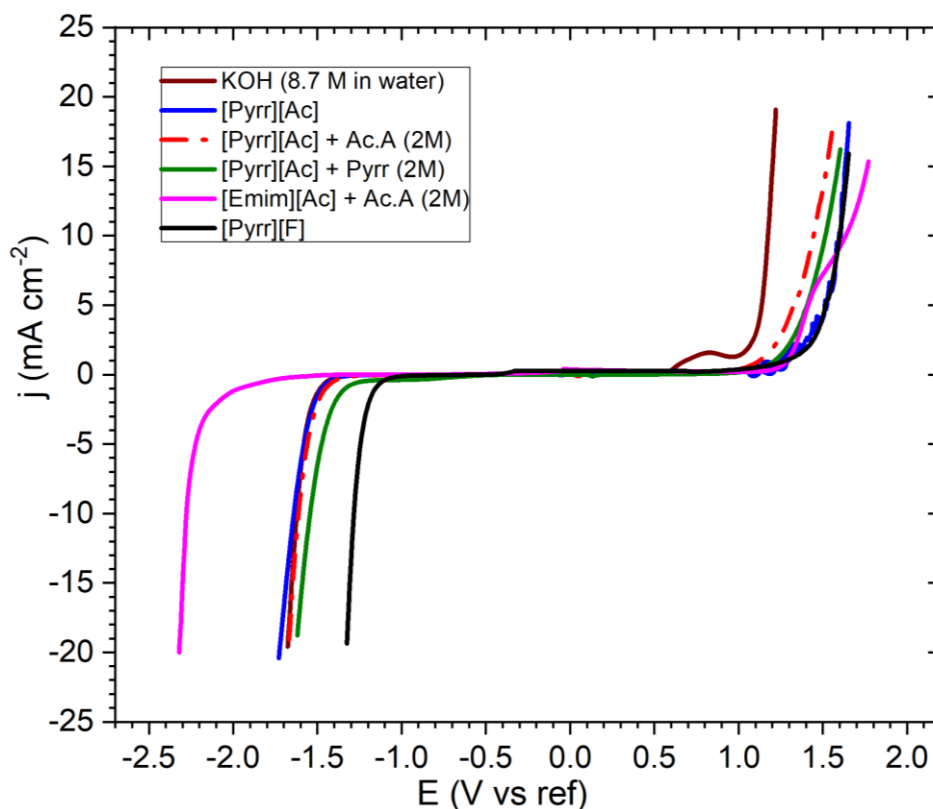


Figure 3 : LSV on gold electrode for the pure ILs and their mixtures at $5 \text{ mV}\cdot\text{s}^{-1}$ at 298 K. The reference electrode was Hg/HgO for KOH solution and Ag/AgNO₃ in IL for the other systems.

The electrochemical windows measured using a cutoff value of $\pm 100 \mu\text{A cm}^{-2}$ are summarized in Table 1. As detailed in supplementary information, Ferrocenemethanol (FcMeOH) could be used as a reference redox probe [17]. Thus, voltammograms of FcMeOH in different media have been used to determine $E^\circ(\text{FcMeOH})$ (Figure S5 and Table S5).

The electrochemical characterization clearly shows that the electrochemical stability window of [EMIM][Ac] + Ac.A (EW: 3.0 V) is larger than that of KOH aqueous solution (EW: 1.9 V), as for [Pyrr][F] (EW: 2.0 V), [Pyrr][Ac] (EW: 2.2 V), [Pyrr][Ac] + Ac.A (EW: 2.3 V) and [Pyrr][Ac] + Pyr (EW: 2.4 V). These ILs are thus attractive for electrochemical applications. Moreover, tiny amount of water does not constrict electrochemical potential windows [18], especially for acetate-based ILs or “water-in-salt” electrolytes [19,20]. The latter can be explained by a strong interaction between water molecules and acetate anions via hydrogen bonds.

Despite [EMIM][Ac]+Ac.A (2M) presents the highest viscosity and the lowest ionic conductivity; it deserves significant interest as electrolyte due to its large EW. Conversely, [Pyrr][F] presents the lowest density and higher ionic conductivity but a moderate EW. Finally, [Pyrr][Ac] and its mixtures with Ac.A and Pyr show intermediate densities and conductivities and an enlarged EW compared to that of KOH. All of these ILs have attractive physico-chemical

properties allowing to consider their use as electrolytes in proton exchange batteries, which has been achieved with a negative electrode in a half-cell configuration.

2.2 Half-Cell Electrochemical Tests

Galvanostatic cycling of the AB_5 electrode was carried out at rates of C/40 and C/10 using ILs and KOH electrolytes, respectively and considering $C = 300 \text{ mAh/g}$. During preliminary tests, it has been observed that, owing to its reducing nature, the formate-based IL ([Pyrr][F]) releases gas in the contact with the AB_5 electrode precluding further studies for this IL.

The galvanostatic potential profiles at the fifth cycle for reversible hydrogen loading of the AB_5 working electrode in different ILs and KOH electrolytes are shown in **Erreur ! Source du renvoi introuvable.** For all electrolytes, a given current was applied for a certain time to complete $300 \text{ mAh}\cdot\text{g}^{-1}$ of charge, which corresponds to the expected capacity of the AB_5 alloy. Looking at the four different media, the charge potentials strongly depend on the electrolyte composition and remain almost constant during the whole charging process. In the half-cell configuration, hydrogen comes from the electrolyte. The charge potential seems therefore related to a single electrochemical reaction which mainly depends on the nature of the electrolyte and therefore of interface reactions. **Thus, the charging potential is tentatively ascribed to the hydrogen evolution reaction (HER), i.e., to the electrolyte acid-base equilibrium to produce hydrogen than can be absorbed by the active material.** If we compare the charge potential for [Pyrr][Ac] and the mixture [Pyrr][Ac]/Ac.A and [Pyrr][Ac]/Pyrr, we can observe the effect of the pH on the HER potential: in the more acidic [Pyrr][Ac]/Ac.A solution, the potential is higher than in pure [Pyrr][Ac], whereas the potential is the lowest in [Pyrr][Ac]/Pyrr. KOH present the highest charge potential, whereas [EMIM][Ac]/Ac.A presents the lowest charge potential, indicating a very different acidity scale for this IL compared to [Pyrr][Ac].

During the discharge step, a plateau is observed in all cases, which can be ascribed to the atomic hydrogen diffusion from the bulk active material to its surface and to its transfer to the electrolyte. The discharge potentials are quite close for the media containing [Pyrr][Ac]. On the contrary, KOH aqueous solution has a lower discharge potential and [EMIM][Ac]/Ac.A shows much higher discharge potential. It may indicate that the nature of the electrolyte is a more important factor regarding the discharge process than the acidity of the medium. During

the discharge process, the mixture of aprotic IL [EMIM][Ac]/Ac.A shows the highest hydrogen release potential, which may be linked to a small proton mobility in this medium due to its high viscosity. However, it is also possible that this IL modifies the material surface, therefore shifting the potential of the hydrogen release.

For [EMIM][Ac]/Ac.A, the huge hysteresis (more than 1 V) between charge and discharge means very low energy efficiency for application. On the contrary, the other ILs and mixtures exhibit lower charge/discharge hysteresis, c.a. 0.3 V to 0.5 V. The latter values are slightly higher than those usually observed in KOH (0.2 V). The lower hysteresis potentials in IL medium were obtained with the mixture of [Pyrr][Ac]/Ac.A (0.3 V) followed by [Pyrr][Ac] (0.45 V). This difference can be attributed to several factors. One of them is the ohmic drop effect induced by the lower ionic conductivity of ILs which is around two orders of magnitude smaller than for 8.7 M KOH aqueous electrolyte [21]. Nevertheless, even with much lower ionic conductivity we can perform charge and discharge in IL media. Other factors are the viscosity and the interface exchange reaction as it is not a simple exchange but an electron – proton exchange.

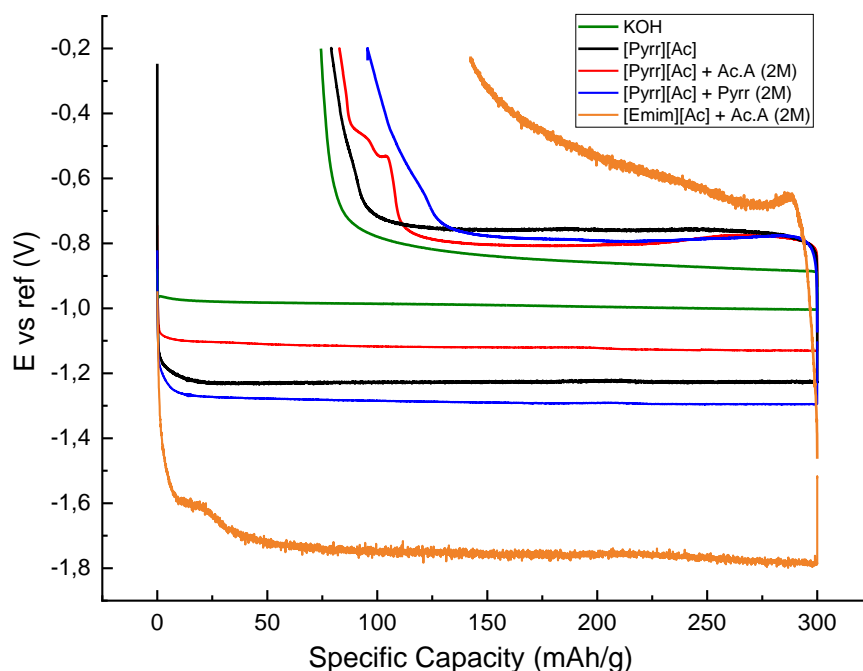


Figure 4 : Galvanostatic titration curves at the 5th cycle of AB₅-type alloy in pure IL, IL/Ac.A mixture, IL/Pyrr mixture and KOH solution. Cycling performed at 25°C using C/40 rate in ILs or their mixtures and using C/10 in KOH solution, respectively.

The specific discharge capacity of the working electrode as a function of the cycle number for the various electrolytes is shown in Figure 5. The highest capacity was obtained using KOH

water-based electrolyte, but several cycles were needed for the alloy activation. The capacity in the [Pyrr][Ac] IL medium and its mixture decreases slowly but without the need of any previous charge/discharge cycle for material activation. It should be noted that the reversible capacity obtained in protic IL [Pyrr][Ac], 220 mAh·g⁻¹, is much higher than that reported by Meng et al., 162 mAh·g⁻¹, obtained at C/100 with an AB₅-type alloy in 2 M acetic acid/[EMIM][Ac] mixture [15]. For the same media a slightly higher capacity, 189 mAh·g⁻¹, was obtained here at C/40.

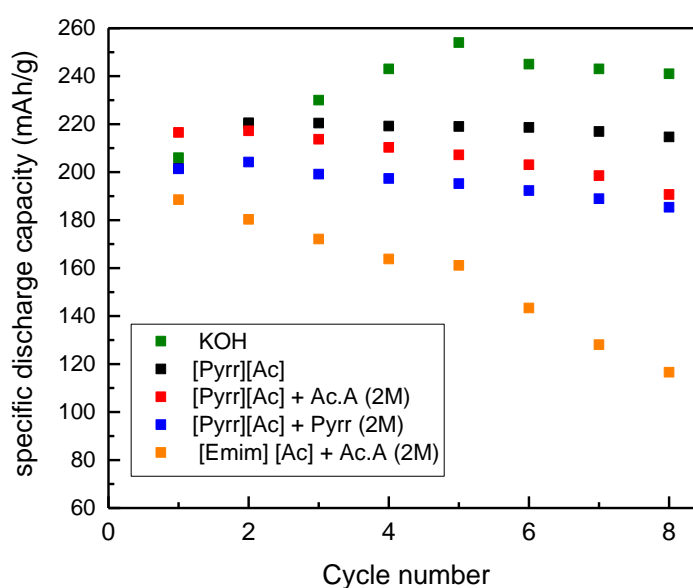


Figure 5 : Specific capacity of the material as a function of the cycle number in different electrolytes.

Table 2 : Maximum capacity, capacity after the 8th cycle, and capacity decrease for the cycling of AB₅ alloy in different electrolytes.

Medium	1 st cycle capacity (mAh.g ⁻¹)	Maximum capacity (mAh.g ⁻¹)	8 th cycle's capacity (mAh.g ⁻¹)	Capacity decrease
KOH	206	254	229	10 %
[Pyrr][Ac]	202	221	215	3%
[Pyrr][Ac] + Ac.A (2M)	217	217	191	12 %
[Pyrr][Ac] + Pyrr (2M)	201	204	185	9 %
[EMIM][Ac]+Ac.A (2M)	189	189	117	38 %

Pyrrrolydinium acetate, [Pyrr][Ac], shows the best electrochemical performance during cycling of the AB₅ alloy and therefore has been selected to perform galvanostatic cycling experiments with different C-rate. Figure 6.a shows the potential profiles of the electrode at different

charge and discharge rates (C/40 and C/20). As expected, the higher the discharge rate, the larger the hysteresis. This can be ascribed to an increase of the ohmic drop due the electrolyte resistance, but also to the necessary reorganization of the IL to accept the proton released from the alloy: at higher C-rate, IL reorganization could increase the hysteresis potential. Another feature of Figure 6b is the decrease of the capacity when increasing the discharge rate. Here again, the capacity can be directly linked to the proton transfer between the electrode and the IL and the IL reorganization needed to solvate the proton (Figure 6.b). It can be noticed that the LSV curve on AB_5 alloy (Figure S6) presents a plateau indicating the stability of the electrolyte, and showing that there is no electrolyte decomposition but an acid-base equilibrium on the negative electrode side. However, due to the half-cell configuration, the electrolyte decomposition may occur at the counter electrode .

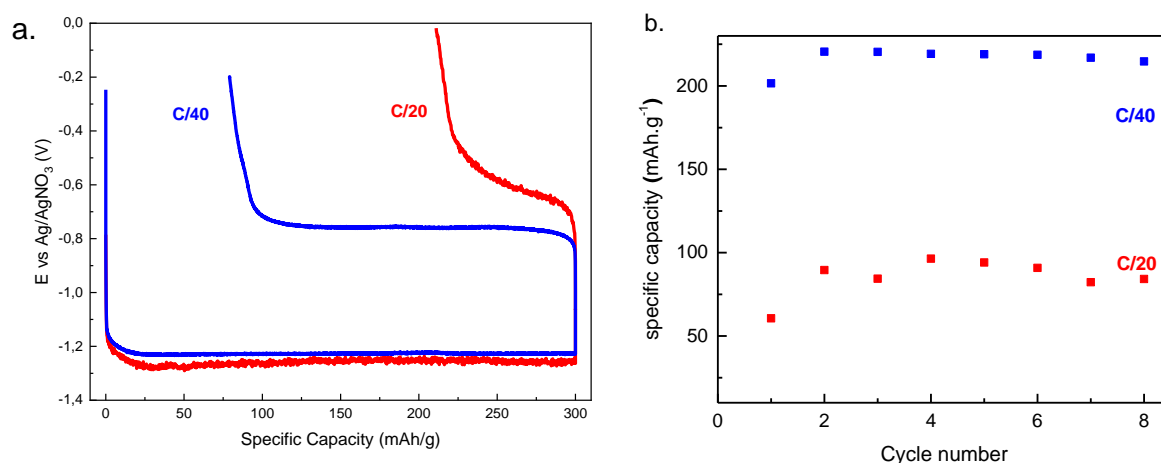


Figure 6 : Galvanostatic potential profiles at different cycling rates (a) and specific capacity as a function of the cycle number (b) on an AB_5 -type alloy in the [Pyr][Ac] electrolyte.

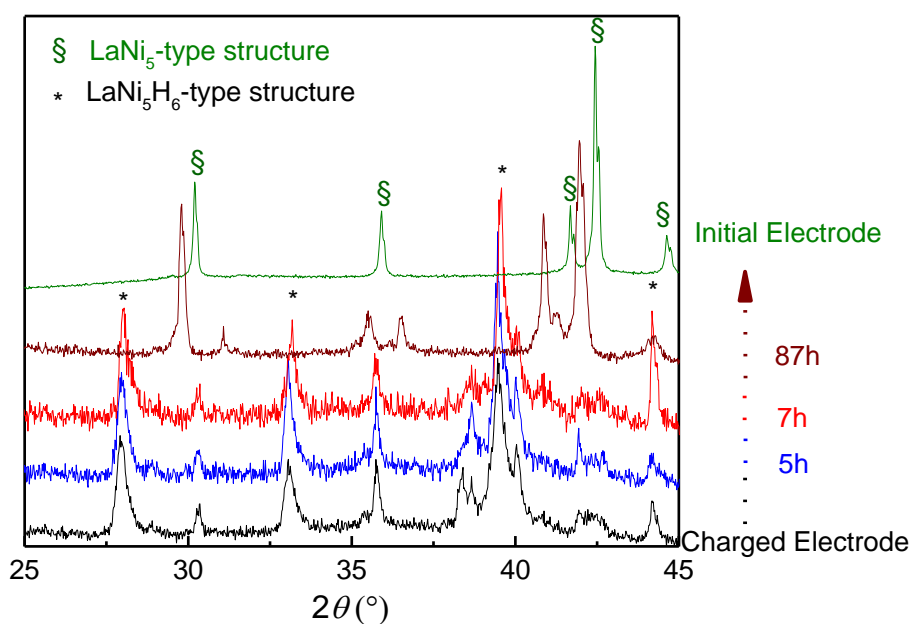


Figure 7 : XRD patterns of the initial electrode, the electrode fully charged in [Pyrr][Ac] medium and time-evolution of XRD patterns of the AB_5 -type electrode during self-discharging in air. Bragg positions of $LaNi_5$ -type structure and $LaNi_5H_6$ -type hydride phase are indicated.

To demonstrate that the electrochemical charging profile leads to the hydrogenation of the electrode, XRD analysis have been performed on the charged electrode. At the end of the galvanostatic charging step, the current was stopped and left at the open-circuit potential. It was observed gas release from electrode inside the IL medium before transferring the sample to the XRD chamber. We ascribe this behavior to the spontaneous hydrogen desorption from the charged electrode, which is a similar behavior than the results reported by Gråsjö about the effect of humidity on hydrogen release [22]. Figure 7 (and Figure S7 for the full 2θ range) shows the XRD patterns of the charged electrode and its evolution as a function of time during XRD recording. The XRD pattern of as-prepared electrode and the Bragg position of $LaNi_5H_6$ -type and $LaNi_5$ -type are indexed. The initial electrode is a single AB_5 phase compound. The charged sample contains the hydride compound as major phase and minor amount the initial intermetallic phase due to the hydrogen desorption. This pattern evolves as a function of the measuring time: the intensity of hydride phase decreases while the intermetallic phase increases. After 87 hours in air, the XRD pattern shows a main intermetallic phase with a small amount of hydrides still present.

3 Conclusions

Two protic ILs [Pyrr][F] and [Pyrr][Ac] have been synthesized. The physicochemical properties of these ILs and their mixtures with acetic acid and pyrrolidine (2 mol L^{-1}) have been studied. The addition of 2M acetic acid or pyrroline shows a decrease of the viscosity and an increase of the ionic conductivity, making them suitable for electrochemical applications.

All these media were used as protic electrolytes to study the electrochemical performance of an AB_5 -type alloy as negative electrode material in a half-cell battery configuration. Screening five different ILs, it was shown that [Pyrr][Ac] possesses the best electrochemical performance with a good cycling stability, moderate charge/discharge overpotentials and a specific capacity of $216 \text{ mAh}\cdot\text{g}^{-1}$.

The obtained results are very encouraging as we demonstrated for the first time that AB_5 -type hydride can be formed in protic ionic liquids. Moreover, this medium enables discharge capacities of AB_5 -compounds close to those obtained in 8.7 M KOH aqueous solution. Moreover, the electrochemical windows of the studied ILs are larger than the one of aqueous KOH solution. It paves the way for working with other negative and positive electrodes with a higher potential difference, and thus leading to larger energy densities.

Acknowledgments

We honor our very dear Michel Latroche who significantly contributed to this scientific project and suddenly passed away.

The authors thank the I-Site FUTURE for the financial support to this work through the IBrHyd Exploratory Project and financial support from IRN-FACES. The authors are also grateful to the ANR toward the H-BAT project (ANR-21-CE50-0030). This work was also supported by the Ecole Doctorale Chimie Physique et Chimie Analytique de Paris Centre (ED 388).

Bibliography

- [1] L. Ouyang, J. Huang, H. Wang, J. Liu, M. Zhu, Progress of hydrogen storage alloys for Ni-MH rechargeable power batteries in electric vehicles: A review, *Materials Chemistry and Physics*. 200 (2017) 164–178. <https://doi.org/10.1016/j.matchemphys.2017.07.002>.
- [2] A. El Kharbachi, O. Zavorotynska, M. Latroche, F. Cuevas, V. Yartys, M. Fichtner, Exploits, advances and challenges benefiting beyond Li-ion battery technologies, *Journal of Alloys and Compounds*. 817 (2020) 153261. <https://doi.org/10.1016/j.jallcom.2019.153261>.

- [3] V. Charbonnier, J. Monnier, J. Zhang, V. Paul-Boncour, S. Joiret, B. Puga, L. Goubault, P. Bernard, M. Latroche, Relationship between H₂ sorption properties and aqueous corrosion mechanisms in A₂Ni₇ hydride forming alloys (A = Y, Gd or Sm), *Journal of Power Sources*. 326 (2016) 146–155. <https://doi.org/10.1016/j.jpowsour.2016.06.126>.
- [4] T. Stettner, A. Balducci, Protic ionic liquids in energy storage devices: past, present and future perspective, *Energy Storage Materials*. 40 (2021) 402–414. <https://doi.org/10.1016/j.ensm.2021.04.036>.
- [5] L. Segade, M. Cabanas, M. Domínguez-Pérez, E. Rilo, S. García-Garabal, M. Turmine, L.M. Varela, V. Gómez-González, B. Docampo-Alvarez, O. Cabeza, Surface and bulk characterisation of mixtures containing alkylammonium nitrates and water or ethanol: Experimental and simulated properties at 298.15K, *Journal of Molecular Liquids*. 222 (2016) 663–670. <https://doi.org/10.1016/j.molliq.2016.07.107>.
- [6] T.L. Greaves, C.J. Drummond, Protic Ionic Liquids: Evolving Structure–Property Relationships and Expanding Applications, *Chem. Rev.* 115 (2015) 11379–11448. <https://doi.org/10.1021/acs.chemrev.5b00158>.
- [7] H. Liu, H. Yu, Ionic liquids for electrochemical energy storage devices applications, *Journal of Materials Science & Technology*. 35 (2019) 674–686. <https://doi.org/10.1016/j.jmst.2018.10.007>.
- [8] T. Stettner, P. Huang, M. Goktas, P. Adelhelm, A. Balducci, Mixtures of glyme and aprotic-protic ionic liquids as electrolytes for energy storage devices, *J. Chem. Phys.* 148 (2018) 193825. <https://doi.org/10.1063/1.5013117>.
- [9] T. Stettner, S. Gehrke, P. Ray, B. Kirchner, A. Balducci, Water in Protic Ionic Liquids: Properties and Use of a New Class of Electrolytes for Energy-Storage Devices, *ChemSusChem*. 12 (2019) 3827–3836. <https://doi.org/10.1002/cssc.201901283>.
- [10] M. Watanabe, M.L. Thomas, S. Zhang, K. Ueno, T. Yasuda, K. Dokko, Application of Ionic Liquids to Energy Storage and Conversion Materials and Devices, *Chem. Rev.* 117 (2017) 7190–7239. <https://doi.org/10.1021/acs.chemrev.6b00504>.
- [11] A. Balducci, Ionic Liquids in Lithium-Ion Batteries, in: B. Kirchner, E. Perlt (Eds.), *Ionic Liquids II*, Springer International Publishing, Cham, 2018: pp. 1–27. https://doi.org/10.1007/978-3-319-89794-3_1.
- [12] A. Eftekhari, Y. Liu, P. Chen, Different roles of ionic liquids in lithium batteries, *Journal of Power Sources*. 334 (2016) 221–239. <https://doi.org/10.1016/j.jpowsour.2016.10.025>.
- [13] S. Shahzad, A. Shah, E. Kowsari, F.J. Iftikhar, A. Nawab, B. Piro, M.S. Akhter, U.A. Rana, Y. Zou, Ionic Liquids as Environmentally Benign Electrolytes for High-Performance Supercapacitors, *Global Challenges*. 3 (2019) 1800023. <https://doi.org/10.1002/gch2.201800023>.
- [14] S. Menne, J. Pires, M. Anouti, A. Balducci, Protic ionic liquids as electrolytes for lithium-ion batteries, *Electrochemistry Communications*. 31 (2013) 39–41. <https://doi.org/10.1016/j.elecom.2013.02.026>.
- [15] T. Meng, K.-H. Young, D.F. Wong, J. Nei, Ionic Liquid-Based Non-Aqueous Electrolytes for Nickel/Metal Hydride Batteries, *Batteries*. 3 (2017) 4. <https://doi.org/10.3390/batteries3010004>.
- [16] R. Khalil, N. Chaabene, M. Azar, I.B. Malham, M. Turmine, Effect of the chain lengthening on transport properties of imidazolium-based ionic liquids, *Fluid Phase Equilibria*. 503 (2020) 112316. <https://doi.org/10.1016/j.fluid.2019.112316>.
- [17] C. Cannes, F. Kanoufi, and A. J. Bard, “Cyclic voltammetry and scanning electrochemical microscopy of ferrocenemethanol at monolayer and bilayer-modified gold electrodes,” *Journal of Electroanalytical Chemistry*, vol. 547, no. 1, pp. 83–91, Apr. 2003, doi: 10.1016/S0022-0728(03)00192-X.
- [18] Y. Zhang, R. Ye, D. Henkensmeier, R. Hempelmann, R. Chen, “Water-in-ionic liquid” solutions towards wide electrochemical stability windows for aqueous rechargeable batteries, *Electrochimica Acta*. 263 (2018) 47–52. <https://doi.org/10.1016/j.electacta.2018.01.050>.

- [19] M.S. Ghazvini, G. Pulletikurthi, T. Cui, C. Kuhl, F. Endres, Electrodeposition of Zinc from 1-ethyl-3-methylimidazolium acetate-water Mixtures: Investigations on the Applicability of the Electrolyte for Zn-Air Batteries, *J. Electrochem. Soc.* 165 (2018) D354.
<https://doi.org/10.1149/2.0181809jes>.
- [20] S. Chen, R. Lan, J. Humphreys, S. Tao, Effect of cation size on alkali acetate-based 'water-in-bisalt' electrolyte and its application in aqueous rechargeable lithium battery, *Applied Materials Today*. 20 (2020) 100728. <https://doi.org/10.1016/j.apmt.2020.100728>.
- [21] R.J. Gilliam, J.W. Graydon, D.W. Kirk, S.J. Thorpe, A review of specific conductivities of potassium hydroxide solutions for various concentrations and temperatures, *International Journal of Hydrogen Energy*. 32 (2007) 359–364.
<https://doi.org/10.1016/j.ijhydene.2006.10.062>.
- [22] L. Gråsjö, G. Hultquist, K.L. Tan, M. Seo, Surface reactions on palladium hydride in vacuum, air and water studied in situ with mass spectrometry, *Applied Surface Science*. 89 (1995) 21–34.
[https://doi.org/10.1016/0169-4332\(95\)00019-4](https://doi.org/10.1016/0169-4332(95)00019-4).